Characterization of Interstitial Hydrogen within Metal Clusters in $Zr_6Cl_{12}H$ and $ZrClO_xH_y$ by Solid-State Nuclear Magnetic Resonance

P. J. Chu, R. P. Ziebarth, J. D. Corbett,* and B. C. Gerstein*

Contribution from Ames Laboratory and the Department of Chemistry, Iowa State University, Ames, Iowa 50011. *Received April 8, 1987*

Abstract: Solid-state NMR studies of hydrogen have been performed on samples of the cluster compound $Zr_6Cl_{12}H$ that contained discernible amounts of the layered compound $ZrClO_xH_y$ ($x + y \leq 1$). The hydrogen in $Zr_6Cl_{12}H$ resonates at 500 ppm upfield from $H_2O(l)$ at 298 K and shows a strong Curie-Weiss paramagnetic shift with temperature but no change in line width, consistent with hydrogen located within an odd-electron and paramagnetic $Zr_6Cl_{12}H$ cluster. Total suppression of this resonance under MREV-8 pulse decoupling indicates that the hydridic species therein experiences random motion on a comparable time scale, in accord with the oversized Zr_6 metal cluster cavity available. These results are consistent with many other observations on other interstitial atoms in Zr_6 octahedral clusters and with the strong correlation of yield with the presence of H_2 in earlier syntheses of several "Zr_6Cl_{12}" phases. The second hydrogen species observed exhibits a broad temperature-independent resonance with center of mass at −5.0 ppm. A variety of nuclear spin dynamic measurements indicate that the primary contributions to this signal come from pairs of hydride with $\bar{d}$(H-H) = 2.5 ± 0.2 Å, and each of these protons interacts to a lesser degree with one or more chlorine atoms at a $\bar{d}$(H-Cl) ≥ 2.7 Å. These parameters and the orientation of the principal axis of the H-H dipole interaction with respect to the shift tensor agree well with the known structure of $ZrClO_xH_y$.

Although the metal cluster phase Zr_6Cl_{12} has been known for some time,[1,2] questions concerning its actual composition and stability as an empty cluster remain. The compound was initially discovered in small amounts following ZrCl–$ZrCl_4$ equilibrations near the composition $ZrCl_2$.[1] The structure deduced by X-ray powder diffraction was identical with that of "Zr_6I_{12}", which is now known to actually be $Zr_6I_{12}C$[3] with carbon centered in the metal cluster.[3,4] However, consistent preparation of Zr_6Cl_{12} was never achieved, and sufficient quantities for physical property measurements were not obtained.

More recently, Imoto and Corbett[5] serendipitously obtained Zr_6Cl_{12}, Zr_6Br_{12}, and the related $M_2ZrCl_6{\cdot}Zr_6Cl_{12}$ (M = Na, K, Cs) by the thermal decomposition of ZrX (X = Cl, Br) in the presence of H_2 and, when appropriate, MCl near 750 °C. Good yields of the clusters were obtained, but these were contaminated by sizeable amounts of inseparable ZrH_{2-x}, the other product. Reactions with Zr:Cl ratios more appropriate to the composition of the cluster phase were not attempted. The greatly improved yields of Zr_6Cl_{12} achieved in the presence of hydrogen and its 0.3% larger lattice parameters compared with those resulting from earlier ZrCl–$ZrCl_4$ reactions[2] led to speculation that Zr_6Cl_{12} might exist both as an empty cluster and as a hydride, similar to Nb_6I_{11} and $Nb_6I_{11}H$.[6]

Solid-state ^1H NMR spectra of small samples of the earlier Zr_6Cl_{12} and $Na_2ZrCl_6{\cdot}Zr_6Cl_{12}$ samples showed only broad Lorentzian-shaped resonances (56–41 kHz at ν_0 = 56 MHz), which were attributed to the ZrH_{2-x} contaminant in the samples. The NMR resonance of ^1H in $ZrH_{1.9}$ was featureless and 55 kHz wide. This dipolar broadened spectrum contrasts with the relatively sharp line observed for noninteractive and immobile protons in hydrogen-centered metal clusters, for example, for the hydrogen centered in the cluster in $CsNb_6I_{11}H$,[7] which shows a single peak 0.6 kHz wide (ν_0 = 35 MHz).[8] Thus, it was concluded on the basis of the NMR evidence that neither cluster sample contained interstitial hydrogen. The greatly improved yields in the presence of hydrogen were attributed to kinetic factors and to the favorable coformation of ZrH_{2-x}. Potential causes for a broad ^1H resonance in other than ZrH_{2-x}, such as from a possibly paramagnetic cluster, were dismissed as was the very broad ESR spectrum observed for only one of two Zr_6Cl_{12} samples at room temperature.[5]

Circumstantial evidence, however, strongly supports the presence of interstitial hydrogen in these phases. The idea that hydrogen could be present is augmented by a great deal of recent experience, which indicates that a large number of other zirconium and scandium chloride cluster phases can be obtained *only* when an interstitial element Be, B, C, ..., is bound in each cluster, raising the cluster-based electron count into the range of 13–16, with 14 electrons being most favored.[3,9-11] Three of the four signs associated with the discovery of these other interstitially stabilized clusters also point to interstitial hydrogen in the Zr_6Cl_{12} phases: low and irregular yields, an otherwise electron-deficient M_6X_{12} cluster (12e), and improved yields upon the addition of the appropriate interstitial element. The fourth sign, a residual electron density in the cluster center from X-ray studies, would not be expected for hydrogen, of course. Preparation of good quality samples appeared to be the key to unraveling the role of hydrogen in the preparation and stability of Zr_6Cl_{12}.

As an abundant spin $I = {}^1/_2$ species, ^1H is easily detectable by NMR, the lower limit of detectability being roughly 10^{17} spins for a line 10 Hz wide.[12] There is a broad range of transient techniques to perturb and control nuclear spin dynamics in order to probe the possible identities of the local surroundings in a solid.[13] The presence of nearby hydrogen atoms is reflected in the homonuclear dipole coupling. Identities of nearest neighbors may also be probed with homo- and heteronuclear scalar and dipolar couplings, utilizing differences in the dependencies of the forms of these couplings on spatial and spin variables and on whether or not one of the partners in the coupling is a spin $^1/_2$ nucleus. Motion of the protons is probed by the response of the proton magnetization to multiple-pulse sequences with cycle times on the order of the motional correlation time.[14] Particularly noteworthy with respect to the last point is the structural evidence that the

(1) Cisar, A., Ph.D. Thesis, Iowa State University, Ames, IA, 1978.
(2) Cisar, A.; Corbett, J. D.; Daake, R. L. *Inorg. Chem.* **1979**, *18*, 836.
(3) Smith, J. D.; Corbett, J. D. *J. Am. Chem. Soc.* **1985**, *107*, 5704.
(4) Fry, C. G.; Smith, J. D.; Gerstein, B. C.; Corbett, J. D. *Inorg. Chem.* **1986**, *25*, 117.
(5) Imoto, H.; Corbett, J. D.; Cisar, A. *Inorg. Chem.* **1981**, *20*, 145.
(6) Simon, A. *Z. Anorg. Allg. Chem.* **1967**, *355*, 311.
(7) Imoto, H.; Corbett, J. D. *Inorg. Chem.* **1980**, *19*, 1241.
(8) Barnes, R. G., Department of Physics, Iowa State University, private communication, 1980.
(9) Ziebarth, R. P.; Corbett, J. D. *J. Am. Chem. Soc.* **1985**, *107*, 4571.
(10) Hwu, S. J.; Corbett, J. D. *J. Solid State Chem.* **1986**, *64*, 331.
(11) Ziebarth, R. P.; Corbett, J. D. *J. Am. Chem. Soc.* **1987**, *109*, 4844.
(12) Becker, E. D. *High Resolution NMR*; Academic: New York, 1980.
(13) Gerstein, B. C.; Dybosky, C. R. *Transient Techniques in NMR of Solids*; Academic: New York, 1985; Chapter 3.
(14) Reference 13, Chapter 5, Section VI.

0002-7863/88/1510-5324$01.50/0

octahedral cavity in Zr_6Cl_{12} (as measured in $K_2ZrCl_6 \cdot Zr_6Cl_{12}$[5]) is considerably oversized for a hydrogen; viz., $d(Zr-H) \simeq 2.26$ Å here vs. 2.08 Å in ZrH_2 and 2.10 Å in Zr_2Br_2H, both with four-coordinate hydrogen.[15]

In the present work, the anisotropic shielding and the homonuclear dipolar and heteronuclear dipolar interactions are all used to help identify the nature of hydrogen in the system under study. These were studied under variable magnetic fields with and without sample spinning, with spinning on or off the magic angle, and with spin dynamics that selectively remove anisotropic shielding and homonuclear dipolar interactions. In addition, the presence of proton motion on the order of multiple pulse cycle times is probed by the response of protons to homonuclear decoupling sequences. The results represent a model study in which a broad range of spin and space rotations and anisotropic interactions have been exploited to probe hydrogen in the solid state and to assist in the determination of structure.

Experimental Section

Materials. Because of their air- and moisture-sensitive nature, all products and reactants were handled under an inert atmosphere or under vacuum. Zirconium powder and $ZrCl_4$ were prepared as previously described.[3] Hydrogen was introduced into the reactions in the form of $ZrH_{1.8}$, the composition of which was calculated from the initial zirconium weight and the change in pressure of the known volume of hydrogen used in the synthesis.

Syntheses. The reactivity of reduced zirconium halides with fused silica at temperatures sufficient for cluster formation (>600 °C) necessitated the use of welded Ta containers encapsulated in evacuated and sealed fused-silica jackets. Samples of $Zr_6Cl_{12}H$ were prepared by the reaction of Zr powder (>100 mesh), $ZrCl_4$, and $ZrH_{1.8}$ at 700 °C over a 2–3-week period. Sample A, used to obtain all the spectra shown, was prepared from a reaction stoichiometry with a Zr:Cl:H ratio of 6:12:4. Excess $ZrCl_4$ sufficient to give approximately 5 atm at 700 °C was also included to reduce disproportionation of the desired cluster compound at this temperature. The yield of $Zr_6Cl_{12}H$ was estimated from relative intensities in the Guinier powder diffraction pattern to be on the order of 90%, although a microscopic examination of the product suggested it might be 5–10% lower. (This assessment excludes the excess $ZrCl_4$ that was first sublimed off under dynamic vacuum at 250 °C.) The other phase present was identified as $ZrClO_xH_y$ ($0 < x < 0.43$, $x + y \leq 1$) in a ZrCl-type structure[16,17] based on line positions, intensities, and lattice constants determined from Guinier powder diffraction ($a = 3.4854$ (5) Å, $c = 27.04$ (2) Å). The identification of this oxygen-containing species correlates with the line-shape and heteronuclear dipolar coupling analyses and the proton spin counting in the NMR experiments. The excess hydrogen used in the $Zr_6Cl_{12}H$ synthesis was presumably partially taken up by both the Ta tube and this second oxide phase.

Sample B was prepared under similar conditions with a Zr:Cl:H ratio of 6:12:1.8. The yield of $Zr_6Cl_{12}H$ was marginally lower than reaction A (≃5%), with a slightly hydrogen-poorer $ZrClO_xH_y$ (ZrCl-type structure) making up the difference. The assignment of $ZrClO_xH_y$ as the second phase is also consistent with the evidence obtained for a third sample C prepared similarly from a mixture with a Zr:Cl:H ratio of 6:12:1.8 and ≃10 atm equivalent excess of $ZrCl_4$ that was further hydrogenated at 200 °C in a Mo boat with 1 atm of H_2. The small sample size and large hydrogen volume prevented an accurate measure of the hydrogen uptake. However, the observed conversion of the $ZrClO_xH_y$ from the ZrCl- to ZrBr-type structure is consistent with the previous experimental experience, which showed that the ZrBr structure type is adopted by $ZrClO_xH_y$ when $x + y$ approaches unity.[17] Insufficient data are available to estimate the amount of hydrogen in $ZrClO_xH_y$ in either sample A or B.

NMR Measurements. NMR experiments were performed at 5.2 T in a superconducting magnet and at 1.3 T in an iron-core solenoid magnet with a pulse NMR spectrometer similar to that described earlier.[18] Hydrogen resonates at 220 and 56 MHz, respectively, in these two fields. A total of 32 766 scans was required to obtain a satisfactory signal-to-noise ratio of the transient decay signal. A simple $\pi/2$ pulse was applied with inverse phase cycling (alternate pulses 180° out of phase) in order to minimize base-line artifacts from pulse breakthrough and ringing. A longitudinal relaxation time measured by progressive saturation yielded a value of roughly 0.1 s at 220 MHz and slightly less at 56 MHz. A repetition rate of 0.5 s was therefore used for most of the experiments. An aqueous $FeCl_3$ solution was used for tuning and as a reference at both fields. Variable-temperature experiments were performed on a home-built cryogenic system with a Varian V-4343 temperature controller to regulate the N_2 flow rate and the temperature.

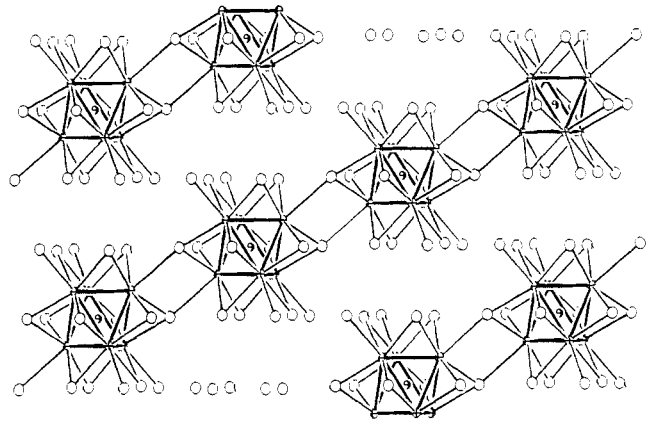

Figure 1. [110] projection of the structure of the $Zr_6Cl_{12}H$ with zirconium octahedra in heavy outline. The proton is believed to occupy the center of the Zr_6 clusters.

Variable-angle sample spinning experiments were performed with a home-built CRAMPS probe[19] using a Gay type[20] rotor (2 kHz). The magic angle was adjusted by utilizing the Pake doublet feature of the spectrum of powdered $CaSO_4 \cdot 2H_2O$. The rotation angle θ was measured from the scaled Pake doublet of the rotational sidebands according to eq 1 where ΔB is the splitting of the scaled Pake doublet of single rotational

$$\Delta B = ((3\cos^2(\theta - 1))/2)\omega_D = P_2(\cos\theta)\omega_D \quad (1)$$

sideband and ω_D is the splitting of the static Pake doublet spectrum. A single sharp center peak (MAS) will appear if $3\cos^2(\theta - 1) = 0$ is satisfied.

Multiple-pulse experiments were performed as described previously.[13] The MREV-8 pulse cycle time was 36 μs after maximizing the power. The scaling factor under this experiment was determined by the response of H_2O at several off-resonance frequencies.[14] Proton spin counting measurement was accomplished by comparing the zero-time free induction decay (FID) between the samples and a distilled water reference.

NMR data are presented on either the σ scale, with increasing σ value corresponding to higher field, or in kilohertz units where more negative shift values are at higher field.

Structure Description. The heavy-atom structure of $Zr_6Cl_{12}H$ has been shown by Guinier powder diffraction to be that of $Zr_6I_{12}C$.[3,5] As shown in Figure 1, the principal building block is the Zr_6Cl_{12} cluster, a trigonal-antiprismatic Zr_6 core surrounded by 12 chlorine atoms that bridge each of the 12 edges. The structure is a cubic close-packed array of these Zr_6Cl_{12} clusters with the $\bar{3}$ axis of each cluster along $\vec{c}$ and normal to the layer direction. The six chlorine atoms around the waist edges that lie in the same (puckered) layer serve as more distant terminal chlorine atoms to metal vertices on six adjacent clusters, three above and three below. A hydrogen atom presumably is bound within each Zr_6Cl_{12} cluster, similar to that for the carbon atom in $Zr_6I_{12}C$ and hydrogen in $Nb_6I_{11}H$. PES, dimensional, and theoretical evidence indicate the hydrogen in such electron-rich environments should be considered hydridic in character.[21]

A $ZrClO_x$ phase is known to form via continuous random insertion of oxygen into tetrahedral metal interstices in the 3R-ZrCl, a structure in which tightly bound slabs are formed from cubic closed-packed homoatomic layers sequenced Cl–Zr–Zr–Cl.[16] The oxide derivative has subsequently been found to take up hydrogen as $ZrClO_xH_y$, evidently utilizing the remaining tetrahedral sites, to an experimentally determined limit of $x + y \simeq 1.0$.[17] (Different hydride structures are formed in the absence of oxygen.[15]) The stacking of these slabs is found to change from ZrCl- to ZrBr-type as $x + y$ approaches 1.0, but this difference is not significant as far as ^1H NMR results.

Results and Discussion

The Fourier transforms of the free induction decays obtained by applying a simple $\pi/2$ pulse to sample A ($Zr_6Cl_{12}H$ +

(15) Wijeyesekera, S. D.; Corbett, J. D. *Inorg. Chem.* **1986**, *25*, 4709.
(16) Seaverson, L. M.; Corbett, J. D. *Inorg. Chem.* **1983**, *22*, 3203.
(17) Wijeyesekera, S. D.; Corbett, J. D., unpublished research.
(18) Cheung, T. T. P.; Worthington, L. E.; Murphy, P. D.; Gerstein, B. C. *J. Magn. Reson.* **1980**, *41*, 158.
(19) Gerstein, B. C. *Philos. Trans. R. Soc. London, A* **1981**, *No. 299*, 521.
(20) Gay, I. D. *J. Magn. Reson.* **1984**, *58*, 413.
(21) Corbett, J. D.; Marek, H. S. *Inorg. Chem.* **1983**, *22*, 3194.

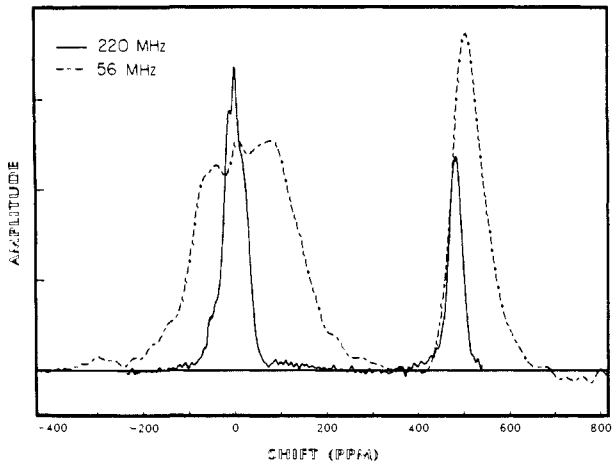

Figure 2. ^1H NMR spectrum for the $Zr_6Cl_{12}H + ZrClO_xH_y$ samples at 220 and 56 MHz. Notice the large upfield shift at approximately 500 ppm. The reference is $Fe^{3+}(aq)$.

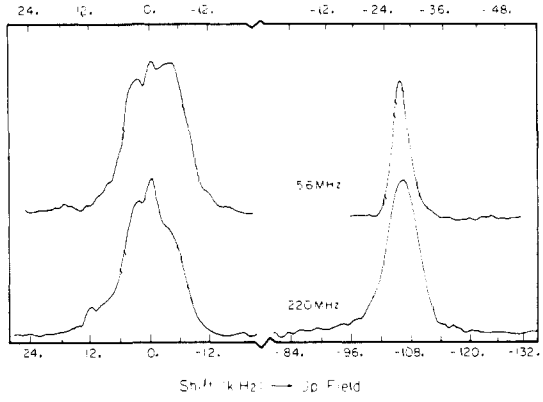

Figure 3. ^1H NMR spectrum of Figure 1 redrawn in kilohertz units to demonstrate the relative line widths. The 56.0-MHz spectra correspond to the top scale. The upfield peak shows a good fit to a Gaussian line shape. The downfield spectra show features of mutually oriented dipolar and chemical shift interactions.

$ZrClO_xH_y$) at two different magnetic fields are shown in Figure 2. Two peaks were resolved at both fields. The centers of mass of the two peaks are at −5.0 ppm and approximately 500 ppm as referenced to $Fe^{3+}(aq)$. The relative ratios of the two hydrogen species inferred from the integrated area of the −5.0 and 500 ppm absorptions are 2.0 to 1.0 for sample A, about 2.2 to 1 for sample B, and 4.2 ± 0.4 to 1 for sample C, indicating that an increasing amount of the $ZrClO_xH_y$ phase was produced as the preparation proceeded from A to C. Of particular importance is the recognition that the measurements were performed on a two-phase mixture, with rather different properties of hydrogen in the two phases. In the following, the NMR spectra of the upfield and the downfield components are discussed individually and identified with $Zr_6Cl_{12}H$ and $ZrClO_xH_y$, respectively.

Upfield Component, $Zr_6Cl_{12}H$. The effective transverse relaxation time T_2^* of the upfield peak was determined by nonlinear least-squares fitting of the spectrum to various line-shape functions.[22] The Gaussian function seemed to yield the best fit for the spectra taken at both magnetic fields, implying that this peak is homogeneously broadened (vide infra), and yielded relaxation times of 81 ± 9 and 52.5 ± 2 μs at 56 and 220 MHz, respectively. The spectra are redrawn in Figure 3 in kilohertz units for better comparison of the line shape and the line width.

Magic angle spinning (MAS) reduces the line width at 220 MHz only slightly and reveals no rotational sidebands, indicating that the limiting line width from homogeneous broadening is approximately 5.5 kHz (T_2 = 80 μs). This result correlates with

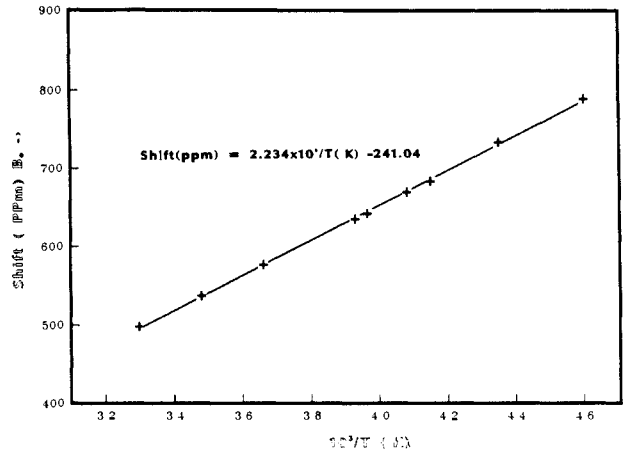

Figure 4. Temperature variation of the shift of the upfield peak between 218 and 298 K. The linear relation with T^{-1} is characteristic of a Curie–Weiss paramagnetic shift of a proton coupled to an unpaired electron.

the fact that the line width of this peak at 56 MHz (4.7 kHz) is not one-fourth of that taken at 220 MHz (7.5 kHz), as would be expected for an inhomogeneously broadened shift interaction.

The upfield peak is totally suppressed on MREV-8 multiple-pulse homonuclear decoupling.[19] This phenomenon has been found in several other systems undergoing rapid nuclear motion where the effective magnetization changes owing to the motion of the nuclei is on a time scale on the order of the sampling time of the multiple-pulse sequence (18 μs).[14,19] As a result, the transient signal is not coherently averaged in the stroboscopic observation windows. This behavior supports the idea that the proton in this environment is undergoing motion.

The potential origins of the large upfield shift are now considered. The theoretical basis for the screening effect of paired electrons was initially formulated by Ramsey[23] and developed for the case of protons by Lau and Vaughn.[24] To observe the high upfield shift within this model, the diamagnetic term σ_d must significantly override the paramagnetic term σ_p. The rapid hopping of the proton within the cluster inferred from multiple-pulse experiment allows us to consider only the isotropic value in Ramsey's formula. This shift should be independent of temperature in view of the implied temperature independence of the wave functions. Another potential origin of the upfield shift is through coupling with an unpaired electron spin. Addition of a hydrogen atom to the empty, 12e Zr_6Cl_{12} cluster would result in an unpaired electron configuration, probably deriving from a hole in the metal-based t_{2g} or t_{1u} orbital set.[3] Unpaired electron density in the ground state would produce a strong local magnetic field and give a chemical shift to the hydrogen nucleus that is orders of magnitude larger than the shift usually observed in diamagnetic molecules.

When the mean value of the electron magnetic moment $\langle S_z \rangle$ is related to the bulk Curie Law magnetic susceptibility,[25,26] the magnitude of the shift associated with the unpaired electronic spin density in the ground state of the $Zr_6Cl_{12}H_x$ cluster can be found to equal

$$\Delta H/H = (g\beta/\gamma\hbar)[a(S + 1)S/3KT]$$

Substituting appropriate constants and units yields eq 2 where

$$\Delta H/H = 0.01053a(S + 1)S/T \qquad (2)$$

a is the hyperfine coupling constant in units of megahertz. Figure 4 shows that this peak shifts further upfield as the temperature is decreased from 298 to 218 K, the linear least-squares fit cor-

(22) Chu, P. J. *Manual for Interactive Eight-Peak Fitting*, Ames Laboratory Report, Jan 1986.

(23) Ramsey, N. *Phys. Rev.* **1950**, *78*, 699.
(24) Lau, K. F.; Vaughn, R. W. *Chem. Phys. Lett.* **1975**, *33*, 550.
(25) Jesson, J. In *NMR of Paramagnetic Molecules*; La Mar, G., Horrocks, W., Holm, R., Eds.; Academic: New York, 1973; Chapter 1.
(26) Carrington, A.; McLachlan, A. *Introduction to Magnetic Resonance*; Harper & Row: New York, 1967; Chapter 13.

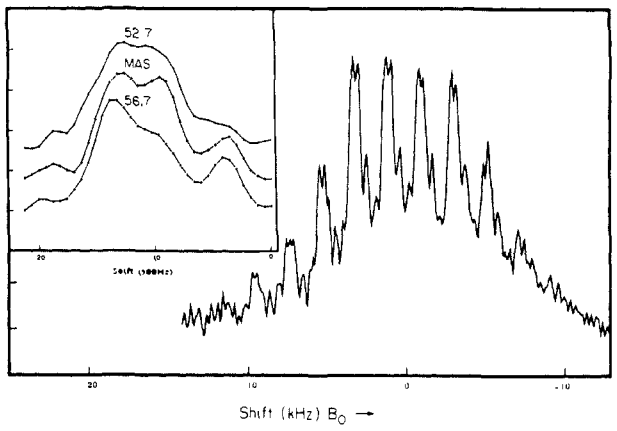

Figure 5. MAS spectra at 220 MHz with spinning speed smaller than the anisotropy. The inset shows the change of the center band with sample spinning at 52.7°, 54.7°, and 56.7° with respect to the magnetic field.

responding to a slope of 2.234×10^5 ppm K and an intercept of −241.04 ppm. The linear behavior indicates that the upfield peak is associated with a Curie Law type magnetic susceptibility, and the presence of unpaired electrons in the ground state is thus confirmed.

The difference of ~16 ppm in the shifts of the two upfield peaks shown in Figure 2 is related to the fact that the experiments were performed at different ambient temperatures, 19 °C (ν_0 = 56 MHz) and 25 °C (ν_0 = 220 MHz). A difference of 15.4 ppm is calculated from the above inverse-temperature relationship.

The slope of the $(\Delta H/H)$ vs T^{-1} curve (Figure 4) leads to a hyperfine coupling constant of 28.29 MHz or 6.64 kG, a value quite typical of organic radicals.[25] This shift can be related to the unpaired electron density at the nucleus of the hydride, $\rho(N)$. According to Fermi's formula, $\rho(N)$ is determined to be 4.27×10^{22} e/cm^3, which amounts to 0.02 times the unpaired electron density found at the nucleus of an isolated hydrogen atom.[25,26]

The above results indicate that the upfield hydrogen species resides in the environment of unpaired and localized electrons and is highly mobile at room temperature. It is therefore reasonable to locate the hydrogen inside the octahedral zirconium cluster. Both the rapid proton motion and the temperature dependence of the shift are supportive of the hypothesis regarding the formation and stability of Zr_6Cl_{12} (cf. Introduction), namely, that hydrogen is needed for its synthesis and, as with all other examples of $Zr_6Cl_{12}Z$ clusters, the interstitial non-metal Z atom contributes both electrons and bonding to the cluster.[9] In the particular case of $Zr_6Cl_{12}H$, the cavity size is determined largely by the Zr–Zr bonding with 11 electrons in metal–metal bonding t_{2g} and t_{1u} sets (in the octahedral limit).[3] This leaves $\bar{d}$(Zr–H) ≃ 2.26 Å, at least 0.15 Å too large for optimal bonding,[5,15] a fact that is reflected in the rapid motion of hydrogen within the metal cluster.

Downfield Component, $ZrClO_xH_y$. There are several features in the MAS spectrum of the downfield component (Figure 5) from which the major Hamiltonians affecting the investigated nuclei can be determined. The bulk shape of the spectrum resembles that of a Pake doublet, as expected if the spectrum were inhomogeneously broadened by two-body homonuclear dipolar interactions. The skewed intensity of the rotational sideband under MAS indicates an asymmetric interaction, e.g. chemical shift anisotropy.

Under rapid sample spinning, each rotational sideband splits into four peaks. Three possible conditions may be responsible: (a) more than one hydrogen species with different isotropic shifts; (b) an incorrect setting of the magic angle; or (c) the presence of another interaction that is not scaled by $P_2(\cos\theta)$. The relative intensities and locations of the split peaks are reproduced in all rotational sidebands, suggesting that the splitting does not originate from different hydridic species with different shifts since sidebands corresponding to species with different anisotropies would produce different relative intensities of the split peaks from one rotational sideband to another. The rotational angle was found to match

Table I. Fitting Parameters for the Two Interactions of the $ZrClO_xH_y$ Peaks

field, MHz	DCP, kHz	δ,[a] kHz	η	α,[b] deg	β, deg
220.15	8.8	5.2	0.55	25.0	60.0
56.03	9.3	1.25	0.6	45.0	55.0

[a] δ average value = −22.9 ppm. [b] The fit is relatively insensitive to the angle α.

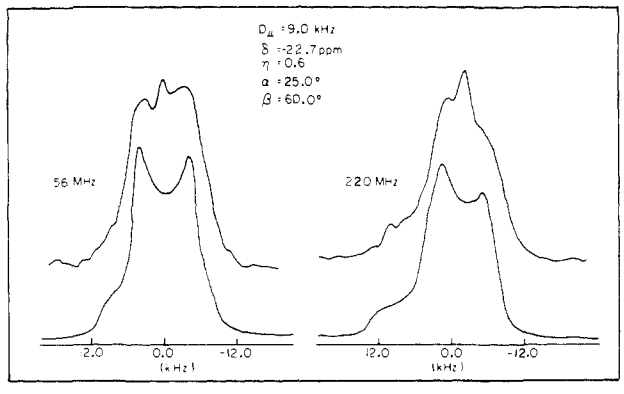

Figure 6. Fitted (bottom) vs experimental (top) spectra of the $ZrClO_xH_y$ component at 220 and 56 MHz. The parameters are those listed in Table I.

the magic angle to within 0.1°. When the sample was spun at ±2° from the magic angle, the splitting of the individual center band (as shown in the inset of Figure 5) did not scale as expected for homonuclear dipolar interactions but rather kept almost constant spacings and changed in the relative intensities. This behavior is characteristic of heteronuclear dipolar coupling between a quadrupolar nucleus and a spin $^1/_2$ nucleus[27] where the scaling upon rotation does not follow $P_2(\cos\theta)$. Therefore, it is concluded that the major contributions to the peak at −5 ppm are homonuclear dipolar interaction and chemical shift interactions with a single isotropic value, plus a heteronuclear dipolar interaction between hydrogen and the quadrupolar chlorine nucleus, that is 1 order of magnitude smaller.

The static line shape of the downfield peak changes with applied field (Figure 3). However, the line width does not scale proportionally, indicative of the presence of a field-independent homonuclear dipolar interaction. Spectra governed by these two interactions depend both on the individual interaction parameters characterizing shielding and dipolar tensors and on the mutual orientation between these two interactions. A line-shape simulation based upon the model of a proton pair experiencing dipolar plus chemical shift interactions has been performed and will be detailed elsewhere.[28] The interaction parameters obtained from the simulation of the spectra at two fields are listed in Table I, and the calculated best-fit spectra are compared with the experimentally observed data in Figure 6. Good agreement is obtained at each field, supporting the assumption that the majority of hydrogen atoms contributing to the downfield peak are isolated hydride pairs with single chemical shifts. From the dipolar coupling constants, the internuclear distance of the dipolar pair is calculated to be 2.5 ± 0.2 Å.

The small component of proton species appearing at the center of the spectrum has been ignored in the line-shape fitting. This peak can be related to either the coupling of a relatively distant third proton to the above-mentioned proton pair or the presence of a small percentage of the protons experiencing equidistant three-proton dipolar coupling, a feature that would be expected in the $ZrClO_xH_y$ structure (Experimental Section). Notice that the r^{-3} dependence of the dipolar coupling constant implies that a proton twice the distance from the "isolated" pair of hydrogens produced only one-eighth of the dipolar coupling strength and

(27) Zumbylyadis, N.; Henrichs, P. M.; Young, R. H. *J. Chem. Phys.* **1981**, *46*, 257.
(28) Chu, P. J.; Gerstein, B. C., submitted for publication in *J. Chem. Phys.*

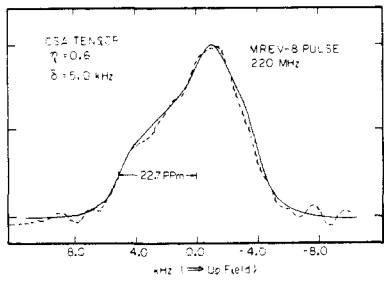

Figure 7. Superposition of a single shielding tensor with a MREV-8 multiple-pulse spectrum (36-μs cycle time). The calculated parameters are $\delta = -22.7$ ppm and $\eta = 0.6$. This spectrum has been corrected for the scaling factor of 1.95.

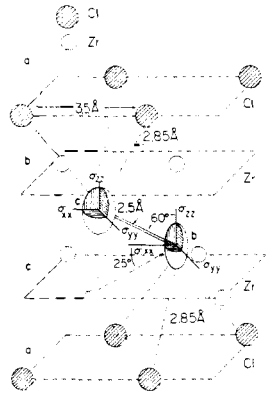

Figure 8. Orientation of the dipolar and the chemical shift interactions of the downfield proton species, $ZrClO_xH_y$. The interproton vector determines the z axis of the axially symmetric dipolar vector. The orientation of these two interactions is seen to be consistent with the structure. Parameters are those listed in Table I from fitting of the static powder spectrum at 220 MHz.

hence can be considered as a remote or isolated hydrogen.

Finally, we applied the MREV-8 multiple-pulse sequence (Figure 7) to suppress the homonuclear dipolar coupling and obtained a tensorlike shielding spectrum for the downfield peak. An anisotropy parameter δ of −22.7 ppm and an asymmetry parameter η of 0.6 gave a good fit to the spectrum, further confirming the line-shape fitting results (Table I).

The foregoing analysis of the static line shape also provides data on the relative orientations of the shielding (Figure 8) and proton–proton dipole tensors that are also in good accord with the structure. The major conduction band electron density is distributed between the metal layers,[21,29] and the shielding tensor axis presumably lies normal to these. The line-shape fitting places the principal proton–proton vector at $(\alpha, \beta) = (25°, 60°)$ with respect to the shielding axis (Table I), nicely consistent with angles of 30° and ~51° found for the midpoint of the tetrahedra in $ZrClO_{0.43}$.[16]

Heteronuclear Dipolar Coupling. The fine features observed in Figure 5 are attributed to the heteronuclear coupling between a quadrupolar nucleus (Cl) and a spin $^1/_2$ nucleus (H). The NMR spectra of a spin $^1/_2$ nuclei affected by dipolar coupling to quadrupolar nuclei have been investigated before.[27,30-33] A single-crystal experiment has shown that heteronuclear dipolar coupling causes an asymmetric splitting of the spin $^1/_2$ spectrum into $2I + 1$ peaks,[31] while for a spinning sample the splitting can appear as a doublet for small values of e^2qQ/ω_o, the ratio of the quadrupolar coupling constant to the Larmor frequency, and up to $2I + 1$ splittings for large values,[30] as observed.

Although an exact calculation was not carried out, a simple approximation has been attempted. Assuming that the "size" of the splitting is basically governed by the strongest coupling in the closest Cl–H pair and that all chlorines coupled to the proton are chemically equivalent, previous calculations[27,33] can be readily applied. The spacing of 950 Hz between the most upfield and most downfield splittings for a spin $^3/_2I$ coupled to a spin $^1/_2S$ nucleus equals 1.6 times that of the dipolar coupling constant, Δ_{Cl-H} (eq 3). From this, we estimate that the internuclear Cl–H distance is roughly 2.7 Å, a lower limit as we have assumed the strongest coupling case.

$$\Delta_{Cl-H} = \gamma_{Cl}\gamma_H\hbar/r_{Cl-H}^3 = 11.77\ (\text{kHz}\cdot\text{Å}^3)\ r_{Cl-H}^{-3} \quad (3)$$

Identity of the Downfield Species. This downfield signal evidently arises from a small amount of the hydrogen-richer second phase in the sample that was identified by X-rays as $ZrClO_xH_y$ ($x < 0.4$, $x + y \leq 1$). This phase has a close-packed, layered structure sequenced Cl–Zr–Zr–Cl with oxygen and hydrogen distributed randomly over the tetrahedral sites between the zirconium layers.[16,17] These sites fall naturally into two layers, with sites within each layer separated by 3.48 Å, the same as for Zr and Cl, while the interlayer separation of the midpoints of the (compressed) zirconium tetrahedra is 2.605 Å in the refined structure of the host lattice $ZrClO_{0.43}$.[16] The assignment of the downfield NMR peak to this phase is supported by several results: (a) The closest hydrogen–hydrogen separation deduced from the powder line-shape simulation, 2.5 ± 0.2 Å, is very consistent with the 2.60-Å value in the parent $ZrClO_{0.43}$. (b) A lower limit of 2.7 Å for the hydrogen–chlorine distance estimated from the MAS fine structures is in accord with ~2.85 Å observed in the same structure. (c) The variation of the ratio of the areas of the two proton peaks with increasing hydrogen pressure during synthesis is in agreement with the known properties of the nonstoichiometric $ZrClO_xH_y$ (as is the ultimate ZrCl- to ZrBr-type transition).[17] (d) Finally, the relative orientation of the shielding tensor with respect to the interproton vector is also consistent with the structure.

Interaction and information of the foregoing types can be expected to be found with other hydride examples of the double-metal-layer monohalides, viz., in the analogous $RClH_x$ and $M^1_xRClH_y$ where R is a rare-earth element and only hydrogen occupies the tetrahedral sites.[34]

Conclusion

^{1}H NMR studies on nominal Zr_6Cl_{12} preparations containing a small amount of $ZrClO_xH_y$ impurity reveal the presence of two completely different hydrogen species. The shift of the upfield peak at ≃500 ppm relative to $H_2O(l)$ at ambient temperature shows a linear dependence on inverse temperature, indicating that the shift originates from a coupling of an unpaired electron with the hydrogen nucleus. The local hyperfine splitting is determined to be 28.29 MHz. This hydrogen is located inside the octahedral zirconium cage where a single unpaired electron is predicted for the stoichiometry $Zr_6Cl_{12}H$. The high electronic density within the Zr_6 octahedron and the probable hydridic character of the proton investigated may also contribute to the observed temperature dependence of the shift. Total suppression of the resonance in MREV-8 multiple-pulse experiments and the invariance of the line width to temperature indicate that the proton within the oversize Zr_6 metal cluster must exhibit a rapid random motion with time scale on the order of the 18-μs sampling time of the experiment.

The second hydrogen species, associated with the $ZrClO_xH_y$ impurity, is observed 5.0 ppm downfield with an isotropic value that is independent of temperature. Variable-angle sample spinning spectra show that the peak is composed primarily of three inhomogeneous interactions, namely, the shielding anisotropy, the dipolar interaction between a pair of hydrogens, and the dipolar

(29) Ziebarth, R. P.; Hwu, S.-J.; Corbett, J. D. *J. Am. Chem. Soc.* **1986**, *108*, 2594.
(30) Hexem, J. G.; Frey, M. H.; Opella, S. J. *J. Chem. Phys.* **1982**, *77*, 3847.
(31) Natio, A.; Ganapathy, S.; McDowell, C. A. *J. Magn. Reson.* **1982**, *48*, 367.
(32) Haeberkorn, R. A.; Stark, R. E.; van Willigen, H.; Griffin, R. G. *J. Am. Chem. Soc.* **1981**, *103*, 2534.
(33) Menger, E. M.; Veeman, W. S. *J. Magn. Reson.* **1981**, *46*, 257.
(34) Meyer, G.; Hwu, S.-J.; Wijeyesekera, S.; Corbett, J. D. *Inorg. Chem.* **1986**, *25*, 4811.

interaction between the proton and one or more chlorine nuclei, the last being 1 order of magnitude less than the other two. Line-shape analysis shows that the dipolar splitting between the proton pair is 8.6 ± 0.5 kHz at 220 MHz, yielding a shift anisotropy δ of −22.7 ppm. The proton shielding parameters were further confirmed by homonuclear decoupling. Both the interproton distances, 2.5 ± 0.2 Å, and the orientation of this dipolar interaction with respect to the shift tensor that can be deduced from the data are in good accord with the structure of $ZrClO_xH_y$. Simple line-shape analysis of the heteronuclear dipolar interaction from the MAS rotation sideband shows that the proton pairs are also coupled to one or more equivalent chlorine nuclei with a $\bar{d}$(H–Cl) ~ 2.7 Å, consistent with the known structure of $ZrClO_xH_y$.

Acknowledgment. The NMR part of this research was supported by the U.S. Department of Energy, Office of Basic Energy Sciences, Chemical Sciences Division, under Contract W-7405-Eng.82. The synthetic and structural portion (R.P.Z.) was supported by the National Science Foundation, Solid State Chemistry (Grant DMR-8318616), and was also performed in the facilities of the Ames Laboratory, DOE.

Spectroscopic Studies on Ferrous Non-Heme Iron Active Sites: Magnetic Circular Dichroism of Mononuclear Fe Sites in Superoxide Dismutase and Lipoxygenase

James W. Whittaker[†] and Edward I. Solomon*

Contribution from the Department of Chemistry, Stanford University, Stanford, California 94305. *Received July 31, 1987*

Abstract: The geometric and electronic structures of ferrous active sites in Fe superoxide dismutase (FeSD) and soybean lipoxygenase (SBL) have been probed by a combination of optical absorption, circular dichroism, and magnetic circular dichroism spectroscopies in the near-IR spectral region. Distinct ligand field excited state spectra have been observed for the two ferrous proteins, indicating significant differences in active site structures. Temperature and magnetic field dependent MCD intensity for the excited state spectral features have been used to obtain detailed information on the EPR inaccessible ground states in the ferrous complexes. Analysis of the MCD data has provided estimates of ground-state splitting parameters on the two proteins and two ferrous model complexes; the origin of the unusual field dependence of the MCD intensity at saturation has been explained in terms of Zeeman mixing within a $M_S = \pm 2$ non-Kramers doublet which is rhombically split. It is determined that a spin Hamiltonian is not an appropriate description for high-spin ferrous ground-state zero-field splittings for a distorted octahedral or square-pyramidal site. An alternative calculation which includes significant orbital contributions to the ground-state splittings gives the rhombic and Zeeman splittings of the lowest doublet of a ferrous site in terms of spin–orbit coupling within the ligand field split t_{2g} orbitals. This permits quantitative estimates of the t_{2g} d orbital splittings from the MCD intensity data. The ground- and excited-state d orbital splittings have been interpreted in terms of geometric and electronic structures for the active site ferrous complexes: for FeSD, a five-coordinate structure and an effective distorted square pyramidal electronic symmetry is indicated by the experimental data, while for SBL a rhombically distorted roughly octahedral six-coordinate structure is determined. Development of ground- and excited-state probes of the ferrous environments in the enzyme active sites has allowed the interaction of the ferrous sites with small molecules to be studied spectroscopically. The ferrous sites in these two proteins appear to be inaccessible to exogenous ligands, which is significant with respect to their O_2 reactivity in catalysis.

Non-heme Fe centers have been identified as the catalytic active sites in a large number of enzymes whose mechanisms involve interactions of dioxygen with a ferrous site.[1] Typically both ferric and ferrous oxidation states are accessible in these systems, in which the native enzyme may stabilize the ferrous oxidation state. These non-heme Fe proteins may be characterized by the number of interacting iron centers in the active site. Mononuclear Fe sites contain a single metal ion coordinated to the protein. This type of active site is observed in the enzymes Fe superoxide dismutase (FeSD),[2] soybean lipoxygenase (SBL),[3] phenylalanine hydroxylase (PAH),[4] catechol 2,3-dioxygenase (2,3-CTD), etc.[5] These enzymes respectively catalyze the dismutation of superoxide, hydroperoxidation of unsaturated lipids, aromatic ring hydroxylation, and catechol ring cleavage. A second class of non-heme Fe active sites contains a bridged binuclear Fe complex and is found for example in the oxygen carrier protein hemerythrin, where dioxygen reversibly binds to the binuclear ferrous unit, forming a binuclear ferric peroxide complex.[6]

Detailed structural studies are emerging for representative Fe sites of both mono and binuclear types. Crystal structures of the native ferric active site of FeSD from *Ps. ovalis*[7] and *E. coli*[8] have been reported, including one anion complex. These structures are currently at 3 Å resolution and are awaiting completion of the protein sequence for refinement. Various interpretations of the electron density map at the current resolution have been presented; most recently a five-coordinate trigonal-bipyramidal site structure has been proposed for the *E. coli* Fe site.[9] A crystal structure

[†] Present address: Department of Chemistry, Carnegie Mellon University, Pittsburgh, PA 15213.

(1) Hayaishi, O.; Nozaki, M.; Abbott, M. In *The Enzymes*, 3rd ed.; Boyer, P. D., Ed.; Academic: New York, 1970.
(2) Slykehouse, T. O.; Fee, J. A. *J. Biol. Chem.* **1976**, *251*, 5472–5477.
(3) Veldink, G. A.; Vliegenthart, J. F. G.; Boldingh, J. *Prog. Chem. Fats Other Lipids* **1977**, *15*, 131–161.
(4) Gottschall, D. W.; Dietrich, R. F.; Benkovic, S. J.; Shiman, R. *J. Biol. Chem.* **1982**, *257*, 845–849.
(5) Nozaki, M.; Kagamiyama, H.; Hayaishi, O. *Biochem. Z.* **1963**, *338*, 582–590.
(6) (a) Okamura, M. Y.; Klotz, I. M. In *Inorganic Biochemistry*; Eichorn, G. L., Ed.; Elsevier: Amsterdam, 1973; pp 320–343. (b) Kurtz, D. M., Jr.; Shriver, D. F.; Klotz, I. M. *Coord. Chem. Rev.* **1977**, *24*, 145–178.
(7) Ringe, D.; Petsko, G. A.; Yamakura, F.; Suzuki, K.; Ohmori, D. *Proc. Natl. Acad. Sci. U.S.A.* **1983**, *80*, 3879–3883.
(8) Stallings, W. C.; Powers, T. B.; Pattridge, K. A.; Fee, J. A.; Ludwig, M. L. *Proc. Natl. Acad. Sci. U.S.A.* **1983**, *80*, 3884–3888.
(9) Stallings, W. C.; Pattridge, K. A.; Ludwig, M. L. In *Superoxide and Superoxide Dismutase in Chemistry, Biology, and Medicine*; Rotillo, G., Ed.; Elsevier: New York, 1986.

0002-7863/88/1510-5329$01.50/0